Research Square

Preprints are preliminary reports that have not undergone peer review.
They should not be considered conclusive, used to inform clinical practice,
or referenced by the media as validated information.

Conditioned medium of PC-3 prostate cancer cells affects microRNA, lncRNA, mRNAs and their ceRNA networks in osteoblasts

Jia Shi
The Second Affiliated Hospital of Zhejiang University School of Medicine
Runnan Xu
The Second Affiliated Hospital of Zhejiang University School of Medicine
Wenjie Huang
The Second Affiliated Hospital of Zhejiang University School of Medicine
Shuiyan Zhan
shuiyanz2@163.com

The Second People's Hospital of Quzhou

Research Article

Keywords: prostate cancer, osteoblasts, microRNA, lncRNA, ceRNA

Posted Date: May 25th, 2026

DOI: https://doi.org/10.21203/rs.3.rs-9400834/v1

License: This work is licensed under a Creative Commons Attribution 4.0 International License.
Read Full License

Additional Declarations: No competing interests reported.

Abstract

Prostate carcinoma represents a widespread and highly aggressive neoplasm that commonly gives rise to skeletal metastases during later disease phases. Consequently, deciphering the molecular pathways driving osseous dissemination of this malignancy holds significant clinical value. To address this objective, we established an *in vitro* model simulating bone-seeking behavior of prostate carcinoma cells to examine how this cancer type infiltrates skeletal structures. The osteogenic differentiation potential of osteoblasts was assessed after exposure to prostate cancer-conditioned medium. Comprehensive profiling was conducted for microRNAs (miRNAs), long non-coding RNAs (lncRNAs), and messenger RNAs (mRNAs) within osteoblasts treated with or without PC-3 cell-derived conditioned medium. Subsequent screening identified differentially expressed mRNAs, miRNAs, and lncRNA. Functional enrichment analyses of differentially expressed RNAs were carried out through Gene Ontology (GO) and Kyoto Encyclopedia of Genes and Genomes (KEGG). A competing endogenous RNA (ceRNA) interaction map was constructed based on the differentially expressed RNAs. Finally, key RNAs of ceRNA network map were validated by quantitative real-time PCR (qRT-PCR). Conditioned medium of PC-3 prostate cancer cells markedly inhibited the differentiation of MC3T3-E1 osteoblasts. The expression patterns of 35 mRNAs, 121 miRNAs, and 64 lncRNAs were significantly altered in osteoblasts exposure to PC-3 conditioned medium. We constructed the ceRNA network consisting of 14 mRNAs, 11 miRNAs, and 24 lncRNAs. Experimental validation was successfully completed for all critical miRNAs together with their corresponding mRNA and lncRNA partners. In summary, the study employed bioinformatics tools to establish ceRNA networks involved in prostate cancer bone metastasis, thereby illuminating their modulatory functions in aberrant bone matrix formation induced by prostate cancer and underlying the fundamental molecular machinery involved.

Introduction

Bone maintains electrolyte equilibrium, regulates energy metabolism, and dynamic coordination between modeling and remodeling activities[1]. These processes are primarily mediated by osteoblasts, which drive bone formation, alongside osteoclasts, which mediate bone resorption[2]. Moreover, bone represents one of the most frequent sites of metastasis in cancer. Prostate cancer as one of the predominant sources of oncological mortality among males, displaying a pronounced propensity for disseminating to osseous structures[3]. When prostate cancer cells colonize bone tissue, they interfere with normal remodeling dynamics, leading to skeletal lesions that are frequently associated with severe pain and substantial morbidity[4]. Accordingly, elucidating the mechanisms underlying aberrant osteogenesis and pathological bone formation triggered by prostate cancer bone metastasis is of critical importance[5].

Skeletal involvement in prostate cancer disrupts normal osteoblastic differentiation and contributes to both osteolytic and osteoblastic lesions, ultimately diminishing patients' quality of life[6]. The management of prostate cancer with bone metastases primarily relies on systemic therapies aimed at controlling tumor progression, alleviating skeletal pain, and preventing fractures[7]. These approaches

mainly include combination regimens based on androgen deprivation therapy (ADT), bone-modifying agents, and localized radiotherapy[8]. Radiotherapy and chemotherapy are applied to patients individually or are combined with surgery to prevent local recurrence. However, these treatments are mainly palliative cannot improve survival dramatically, and no standard second-line therapy can be selected [9]. There is an urgent need to elucidate the precise molecular mechanisms underlying bone metastasis in prostate cancer in order to facilitate the development of novel therapeutic strategies. Accumulating evidence indicates that the bone microenvironment—particularly regulatory non-coding RNAs, such as microRNAs (miRNAs) and long non-coding RNAs (lncRNAs)—plays a pivotal role in this process[10].

In the present investigation, MC3T3-E1 osteoblastic cells were exposed to conditioned medium derived from prostate cancer cells. Osteogenic differentiation was subsequently compared under pathological conditions (presence of conditioned medium) and physiological conditions (absence of conditioned medium). High-throughput sequencing was employed to identify differentially expressed mRNAs, miRNAs, and lncRNAs in the pathological group. Finally, bioinformatic analyses were conducted to construct lncRNA–miRNA–mRNA competing endogenous RNA (ceRNA) regulatory networks, and selected targets were validated using quantitative real-time PCR (qRT-PCR).

Materials and methods

Preparation of conditioned medium

Human prostate cancer PC-3 cells (ATCC, VA, USA) were maintained in Dulbecco's modified Eagle medium (DMEM; Invitrogen Life Technologies, CA, USA) supplemented with 10% fetal bovine serum (FBS; Gibco, MA, USA) at 37°C under humidified conditions with 5% CO_2. To obtain conditioned medium, cells were seeded at a density of 1×10^6 cells in 25 cm^2 flasks and cultured until reaching approximately 60–70% confluence. After rinsing twice with phosphate-buffered saline (PBS), the medium was replaced with DMEM containing 1% FBS, followed by incubation for an additional 48 h. The supernatant was collected, defined as crude conditioned medium (CCM), filtered through a 0.2-μm sterile membrane, and stored at − 80°C. Final conditioned medium (CM) was prepared by combining CCM with DMEM at a ratio of 1:4.

PC-3 CM treatment and osteogenic differentiation stimulus

MC3T3-E1 murine calvariae pre-osteoblastic cells was obtained from ATCC Cell Bank (VA, USA). For experiments, cells were used in passages four to six. These cells were cultured in DMEM supplemented with 10% FBS and 1% penicillin–streptomycin in culture plates (Nunc International, Denmark). Once cells reached 80% confluence, they were divided into two groups: a treatment group exposed to PC-3 CM supplemented with 50 μg/mL ascorbic acid, 5 mM β-glycerophosphate, and 2 mM glutamine, and a

control group maintained in standard DMEM medium containing the same additives. The culture medium was renewed every 48 h during the experiment.

Alkaline phosphatase (ALP) activity assay

After CM exposure, ALP activity of MC3T3-E1 cells a were measured. Cells were subjected to lysed on ice in radioimmunoprecipitation assay (RIPA) buffer (Cw Biotech, Beijing, China) with brief ultrasonication. Total protein content was measured using a bicinchoninic acid (BCA) assay kit (Cw Biotech). Alkaline phosphatase (ALP) activity was quantified using a fluorescence-based commercial assay kit (Nanjing Jiancheng Biotechnology Co., Ltd., Nanjing, China), with p-nitrophenyl phosphate serving as the reaction substrate, following the supplier's instructions. Absorbance of the reaction product was recorded at 405 nm to determine enzymatic activity.

RT-qPCR

Total RNA was isolated using the MiniBEST Universal RNA Extraction Kit (TaKaRa, Osaka, Japan) according to the manufacturer's instructions. cDNA was performed using equal RNA inputs with a reverse transcription kit (TaKaRa). RT-PCR was conducted using SYBR Premix Ex Taq (TaKaRa) with gene-specific primers on an Agilent Technologies System (CA, USA). Primer sequences are provided in Tables 1 and 2. The cycling parameters comprised 40 iterations of denaturation at 95°C for 3 s, primer annealing at 58°C for 30 s, and elongation at 72°C for 30 s. GAPDH served as the reference gene for mRNA and lncRNA quantification, whereas U6 was used as the internal control for miRNA analysis. Relative expression levels were calculated using the 2^−ΔΔCt method.

Table 1
Primer sequences of mRNA and lncRNA

mRNA	Primer sequences of mRNA(5’-3’)
Col I	F: TTCTCCTGGCAAAGACGGAC R: CCATCGGTCATGCTCTCTCC
OCN	F: ATGGCTTGAAGACCGCCTAC R: GACAGGGAGGATCAAGTCCC
ALP	F: TGGTCACAGCAGTTGGTAGC R: TAGTCACAATGCCCACGGAC
Prlr	F: AGTCTGGACTCCCTGACCTC R: AGTGGATCCGAGGTACTGCT
Nfatc2	F: CCGCGACTCTATACGAACCC R: CGTGGGATGGAGTGATCTCG
Unc5b	F: CATCCGCATTGCCTACTTGC R: GATGTCTCCAGGGTCAGCAC
Klf2	F: GCCTTCGGTCTTTTCGAGGA R: TTAGGTGCGAGCTCTTGGTG
Prkg2	F: CCCTGAACCGTGACGATGAA R: GCCACTGAGCTCTCTCCGTA
Sorcs2	F: CGTTACCTACCAGCGACCAT R: TGCCTGTGGATCTTTGCGAT
Nuak2	F: ATGGTGCCCTAGTATGGGGT R: GTGTGAACCCAAGTCCCCAA
Arhgap22	F: GTTGCATCCCCTGGTCCTAC R: TCATGGTGCACTGTGTCCTC
Hmga1	F: TTTTAAGCTCCCCTGAGCCG R: TGGGGACATGCTGGGATCTA
Atp8b4	F: GCAGACACGAGGAGTGAACAR: GGTTTGTTTCCCCGTCAAGC
Ecm2	F: CTTCACAAGCAAGTGCCACC R: TCCATCCATGTTCAGACGCA
Fosb	F: CTCCGAACCGGAGACTAAGC R: ACTTGAACTTCACTCGGCCA
Hectd2	F: ACTCTCACAGCAGGTTTTCCT R: GTCTTCGCATAGCCGTCGTA
Il1rl1	F: TCCAGCCCTTCATCTGGGTA R: ATGGTGTGTTCACTAGGCGG
A930016O22Rik	F: ACCAAGAAGTCAGCAGGAGC R: ATCATCCAGGCTTGGTGGTG
Eldr	F: AAAGGAGGCCCAAGTCACT R: AACTCTCGGCCGTCTCAAAG
Gapdh	F: GCCTCCTCCAATTCAACCCT R: CTCGTGGTTCACACCCATCA

Table 2
Primer sequences of miRNA

miRNA	miRBase Accession	miRNA Primer sequences(5'-3')
mmu-miR-370-3p	MIMAT0001095	GAGACCAGGTCACGTCTCTG
mmu-miR-96-5p	MIMAT0000541	TTTGGCACTAGCACATTTTTGCT
mmu-miR-1a-3p	MIMAT0000123	GCGCGTGGAATGTAAAGAAGT
mmu-miR-340-5p	MIMAT0004651	GCGCGTTATAAAGCAATGAGA
mmu-miR-138-5p	MIMAT0000150	GCGAGCTGGTGTTGTGAATC
mmu-miR-134-5p	MIMAT0000146	CGCGTGTGACTGGTTGACCA
mmu-miR-543-3p	MIMAT0003168	CGAAACATTCGCGGTGCA
mmu-miR-466m-3p	MIMAT0014883	TACATACACACATACACACGCA
mmu-miR-382-5p	MIMAT0005855	GCGGAAGTTGTTCGTGGTG
Universal reverse primer		AGTGCAGGGTCCGAGGTATT
U6		F: CTCGCTTCGGCAGCACA R: AACGCTTCACGAATTTGCGT

Western blotting

Total protein was extracted from MC3T3-E1 cells using RIPA lysis buffer (Servicebio, Wuhan, China), and concentrations were determined using a BCA assay. Equal protein amounts were separated via SDS-PAGE and transferred to polyvinylidene fluoride (PVDF) membranes (Millipore, MA, USA). Membranes were blocked with 5% non-fat milk in TBST (Servicebio) for 1.5 hours at room temperature, followed by overnight incubation at 4°C with primary antibodies: Rabbit anti-mouse Col I (1:1000, Abcam, Cambridge, UK), Rabbit anti-mouse Runx2 (1:1000, Abcam), Rabbit anti-mouse BMP2 (1:1000, Abcam), Rabbit anti-mouse β-actin (1:3000, Proteintech, Wuhan, China). After washing, membranes were incubated with peroxidase-conjugated secondary antibodies, Goat anti-Mouse IgG (1:5000, Proteintech) for 1.5 h at room temperature. Protein bands were visualized using enhanced chemiluminescence reagents (Servicebio) and imaged with a Bio-Rad gel documentation system (Bio-Rad, CA, USA). Band intensities were quantified using ImageJ software and normalized to β-actin.

ALP and alizarin red-S staining

For ALP and alizarin red-S staining, cells were rinsed with PBS twice and subsequently fixed in 4% paraformaldehyde at 37˚C for 20 min. ALP staining was carried out using a commercially available kit to determine enzymatic activity, while Alizarin Red S staining was applied to evaluate mineralized matrix

formation (kits purchased from Nanjing Jiancheng Biotechnology Co., Ltd.). The stained specimens were then observed under a light microscope.

Preparation of total RNA and cDNA for small RNA sequencing

Total RNA was extracted using Trizol reagent (Invitrogen; Thermo Fisher Scientific) following the manufacturer's protocol. RNA concentration and purity were determined with a NanoDrop 2000 spectrophotometer (NanoDrop Technologies, DE, USA). Samples meeting quality criteria (A260/A280 > 1.8 and A260/A230 > 2.0) were selected for further analysis. RNA integrity was verified using an Agilent 2200 TapeStation (Agilent Technologies, Chandler, AZ, USA), and only samples with an RNA integrity number equivalent (RINe) greater than 7.0 were retained. For library construction, 3' adapters were ligated to RNA fragments prior to 5' adapter addition. Reverse transcription was then performed, followed by limited-cycle PCR amplification. Size-selected PCR products were purified via polyacrylamide gel electrophoresis using the NEBNext® Multiplex Small RNA Library Prep Kit for Illumina® (New England Biolabs, MA, USA). Library quality was reassessed using the Agilent 2200 TapeStation, and qualified libraries were diluted to 2 pM for clustering on a HiSeq 2500 single-end flow cell. Sequencing (1 × 50 bp) was conducted on an Illumina HiSeq 2500 platform by Ribobio Co., Ltd. (Guangzhou, China).

Preparation of total RNA and cDNA for transcriptome sequencing

Ribosomal RNA was depleted from total RNA samples using the Ribo-Zero rRNA Removal Kit (Illumina, CA, USA), and the remaining RNA was fragmented to an average length of approximately 200 bp. after which the remaining RNA was fragmented to approximately 200 bp. First- and second-strand cDNA synthesis was subsequently performed, followed by adapter ligation and PCR enrichment according to the NEBNext® Ultra™ Directional RNA Library Prep Kit (New England Biolabs, USA). Purified libraries were evaluated with the Agilent 2200 TapeStation and quantified using a Qubit® 2.0 fluorometer (Invitrogen, Life Technologies, NY, USA). Final libraries were adjusted to 10 pM and subjected to paired-end sequencing (2 × 150 bp) on an Illumina HiSeq 3000 system at Ribobio Co., Ltd.

Bioinformatics analysis

Sequencing output files were first processed to generate gene-level count matrices, which were subsequently evaluated with DESeq2 (version 1.34.0). Differential expression was assessed using a statistical framework based on the negative binomial distribution. To correct for multiple hypothesis testing, the Benjamini–Hochberg method was applied to control the false discovery rate, and adjusted *p*-values below 0.05 were regarded as statistically meaningful. Considering the substantial number of identified differentially expressed genes (DEGs), more rigorous filtering criteria ($p < 0.01$ and |fold change (FC)| ≥ 2) were implemented to enhance reliability. In contrast, selection thresholds for differentially expressed microRNAs (miRNAs) and long non-coding RNAs (lncRNAs) were set at $p < 0.05$ with |FC| ≥ 2. To further interpret the biological relevance of DEGs, enrichment analyses were conducted using the

Gene Ontology (GO) and Kyoto Encyclopedia of Genes and Genomes (KEGG) databases, enabling the identification of associated biological processes and signaling pathways.

CeRNA network

Using differential expression profiles as a foundation, putative lncRNA–miRNA interactions were identified with miRanda (http://www.plosbiology.org), pictar (https://pictar.mdc-berlin.de/) and RNAhybrid (http://alk.ibms.sinica.edu.tw). Only interaction pairs consistently predicted by all three tools were retained as reliable lncRNA–miRNA candidates. Because lncRNAs acting as competing endogenous RNAs generally show expression patterns opposite to those of their corresponding miRNAs, only negatively correlated pairs were selected for downstream analysis. Subsequently, significantly dysregulated miRNAs and mRNAs were combined to define miRNA–mRNA regulatory associations. Putative mRNA targets were identified using TargetScan (http://www.targetscan.org), miRDB (http://mirdb.org/) and miRWalk (http://mirwalk.umm.uni-heidelberg.de/), and only shared predictions across these platforms were preserved. Interaction pairs exhibiting inverse expression relationships were incorporated into the network framework. The final lncRNA–miRNA–mRNA regulatory network was generated by integrating validated interaction pairs and was visualized using Cytoscape 3.4.0.

Statistical analysis

All data processing and graphical analyses were carried out with GraphPad Prism version 9.5 (GraphPad Software, CA, USA). Data are expressed as the mean ± standard deviation (SD). Statistical differences between two groups were determined using Student's t-test, whereas comparisons involving multiple groups were analyzed through one-way or two-way analysis of variance (ANOVA), followed by suitable post hoc tests. A two-sided p-value less than 0.05 was considered indicative of statistical significance. Each experiment was performed independently at least three times to ensure reproducibility.

Results

PC-3 CM inhibited osteoblastic differentiation of MC3T3-E1 cells.

Measurement of alkaline phosphatase (ALP) activity demonstrated a significant reduction in enzymatic activity on days 1 and 2 following CM treatment (Fig. 1A). To further assess osteogenic potential, the expression of key differentiation markers was examined. qPCR analysis showed that the expression levels of Col1a1, OCN, and ALP genes were significantly downregulated in cells cultured with PC-3 CM (Fig. 1B). Consistently, Western blot analysis showed decreased protein expression of RUNX2, COL1, and BMP4 in treated MC3T3-E1 cells (Fig. 1C-D). In agreement with these findings, both ALP staining and Alizarin Red S staining demonstrated reduced ALP activity and diminished mineralized matrix formation after CM exposure (Fig. 1E-F).

PC-3 CM resulted in the alterations of mRNAs profiling

Transcriptomic analysis indicated substantial differences in gene expression between CM-treated cells and controls. A total of 26 genes were upregulated, whereas 9 genes were downregulated in MC3T3-E1 cells exposed to PC-3 CM (Fig. 2A). KEGG pathway enrichment analysis identified the top 15 significantly enriched signaling pathways. Notably, pathways related to osteoclast differentiation, PI3K-Akt signaling, and cancer-associated signaling were prominently represented (Fig. 2B). GO enrichment analysis further highlighted biological processes relevant to prostate cancer bone metastasis, including stimulus response, extracellular matrix organization, and protein-binding functions (Fig. 2C).

PC-3 CM alters the miRNA and lncRNA profile.

As shown in Fig. 3, the small RNA sequencing results showed that there were 82 upregulated miRNAs and 39 downregulated miRNAs. As shown in Fig. 4, the mRNA sequencing results showed that there were 35 upregulated lncRNAs and 29 downregulated lncRNAs.

The construction of the ceRNA network.

In addition, a competing endogenous RNA (ceRNA) regulatory network was established based on differentially expressed mRNAs, miRNAs, and lncRNAs. As illustrated in Fig. 5A, 11 differentially expressed miRNAs were identified as central nodes within the network. Meanwhile, 14 differentially expressed mRNAs were considered potential target genes according to predictions from miRDB, PicTar, and RNAhybrid. Furthermore, 24 differentially expressed lncRNAs were selected as candidate miRNA sponges based on analyses using miRanda, PicTar, and RNAhybrid. Notably, the expression patterns of lncRNAs were consistent with those observed for mRNAs.

To further substantiate these results, quantitative PCR (qPCR) validation was conducted on key components of the ceRNA network. A subset comprising 14 mRNAs, 9 miRNAs, and 2 lncRNAs was selected for experimental verification. The findings demonstrated that 10 mRNAs were upregulated while 4 were downregulated; among miRNAs, 4 showed increased expression and 5 were decreased; additionally, both lncRNAs exhibited downregulation. These validation results were in agreement with the sequencing data.

Discussion

Osteoblasts reside along bone surfaces and are primarily responsible for bone matrix synthesis and mineralization. *In vivo*, their activity is tightly regulated by the surrounding microenvironment[11]. In prostate cancer (PCa), skeletal involvement represents the predominant metastatic pattern and is a major determinant of unfavorable clinical outcomes[12]. The establishment of bone metastasis is a complex, multistep cascade that involves detachment of tumor cells from the primary lesion, entry into the bloodstream, survival during circulation, colonization of a pre-metastatic niche, homing to bone marrow, and subsequent proliferation[13, 14]. Although several mechanisms underlying skeletal dissemination have been identified, the full molecular landscape remains incompletely understood. In PCa, signaling axes such as RANK/RANKL[15] and CXCR4/CXCL12[16] axes contribute to metastatic

progression by modulating bone remodeling and facilitating tumor cell recruitment. Nevertheless, the contribution of non-coding RNAs, particularly within competing endogenous RNA (ceRNA) regulatory frameworks, to prostate cancer bone metastasis has not been comprehensively characterized. This study used an *in vitro* model of prostate cancer bone metastasis to perform high-throughput sequencing analysis on osteoblasts. Our aim was to explore the potentially complex molecular mechanisms involving lncRNAs, miRNAs, and key genes in the process of prostate cancer bone metastasis.

Treatment with PC-3–derived conditioned medium (CM) markedly impaired osteogenic differentiation in MC3T3-E1 cells. Altered miRNA and mRNA expression profiles observed following CM exposure suggest their involvement in bone metabolic dysregulation during PCa progression. Specifically, reduced ALP activity, decreased Col I, OCN, and ALP transcript levels, diminished calcium deposition, and lower protein expression of RUNX2, COL1, and BMP4 were detected in the CM-treated ("pathological") group. These findings collectively demonstrate that soluble factors secreted by PC-3 cells suppress osteogenic maturation of MC3T3-E1 cells *in vitro*.

To further clarify the functional implications of differentially expressed genes, GO and KEGG analyses to were conducted. Enrichment results consistently highlighted osteoclast differentiation and the PI3K–AKT signaling cascade as significantly represented pathways. Tumor cells are known to enhance RANKL expression in osteoblasts, thereby promoting osteoclast differentiation[17]. Among regulatory pathways implicated in PCa, PI3K/AKT signaling constitutes a central oncogenic axis[18]. Loss of PTEN function frequently leads to aberrant activation of this pathway, facilitating tumor proliferation, metastatic dissemination, and therapeutic resistance. Experimental models involving PTEN or AKT gene manipulation further support their role in enhancing tumor aggressiveness *in vivo*[19, 20].

The canonical ceRNA model proposes that lncRNAs function as molecular sponges by competitively binding to miRNAs, thereby reducing miRNA-mediated repression of target mRNAs and ultimately promoting mRNA expression [21]. Guided by this framework, differentially expressed mRNAs, miRNAs, and lncRNAs were selected to infer interactions and establish a ceRNA regulatory network. This network was constructed using 14 mRNAs, 11 miRNAs, and 24 lncRNAs. To validate these observations, quantitative real-time PCR (qRT-PCR) was performed, confirming that the key lncRNAs A930016O22Rik and Eldr were markedly downregulated. Moreover, the expression profiles of the selected miRNAs (miR-370-3P, miR-96-5P, miR-1a-3P, miR-340-5P, miR-138-5P, miR-134-5P, miR-543-3P, miR-466m-3P, and miR-382-5P) and mRNAs (Prlr, Nfatc2, Unc5b, Klf2, Prkg2, Sorcs2, Nuak2, Arhgap22, Hmga1, Atp8b4, Ecm2, Fosb, Hectd2, and Il1rl1) were consistent with sequencing data.

Previous research has demonstrated that certain miRNAs within ceRNA networks play crucial roles in prostate cancer bone metastasis. For instance, miR-96-5P[22] and miR-466[23] have been reported to enhance migration and invasion of prostate cancer cells. Interestingly, both miRNAs are also highly expressed in osteoblasts, indicating potential functional significance in the bone microenvironment. In contrast, the involvement of lncRNAs in prostate cancer bone metastasis remains insufficiently characterized, and many lncRNAs within ceRNA networks are still poorly understood. In the present

study, the lncRNA Eldr was identified as significantly upregulated in MC3T3-E1 cells. Elevated ELDR expression has been documented in several malignancies, particularly glioma and head and neck cancers[24]. Its molecular function has been investigated in oral cancer, a major subtype of head and neck cancer[25]. Compared with normal oral keratinocytes, ELDR expression is markedly increased in oral cancer cell lines such as Cal27, JHU029, and JHU022. Functional studies indicate that ELDR overexpression promotes cell proliferation and colony formation, whereas its knockdown suppresses proliferation and induces G1/S phase arrest in these cell lines[26]. These findings suggest that ELDR may serve as an important regulatory lncRNA in prostate cancer bone metastasis.

Currently, substantial evidence supports Paget's "seed and soil" hypothesis, which emphasizes the specific interaction between metastatic prostate cancer cells and the bone microenvironment. Tumor-derived exosomes are recognized as key mediators of microenvironmental remodeling[27]. Cancer cells can release abundant exosomes enriched with miRNAs, lncRNAs, and mRNAs, which can be transferred to recipient cells and modulate their biological functions[28, 29]. In this study, an in vivo model of prostate cancer bone metastasis was established, and differentially expressed miRNAs, lncRNAs, and mRNAs were identified in osteoblasts. These molecules may be delivered via exosomes secreted by prostate cancer cells.

Despite these findings, several limitations should be considered. First, the sample size was relatively limited, and larger cohorts are required for further validation. Second, commonly used prostate cancer cell lines include PC3, DU145, and LNCaP[30]. while hFOB 1.19 and MC3T3-E1 are widely utilized for osteogenic differentiation studies[31]. Although MC3T3-E1 cells were employed in this study based on prior research, future investigations should incorporate multiple prostate cancer and osteoblast cell lines, particularly those of human origin. Finally, although the ceRNA network was established and key lncRNAs with dynamic expression patterns were identified, their precise roles in regulating osteogenesis remain unclear. Additional functional experiments, such as gene overexpression or knockdown assays, are necessary to clarify their involvement in prostate cancer bone metastasis.

Declarations

Ethics approval and consent to participate

Not applicable.

Patient consent for publication

Not applicable.

Competing interests

The authors declare that they have no competing interest.

Funding

This study was supported by the National Natural Science Foundation of China (No. 82575053).

Author Contribution

JS designed the study, analyzed the data, performed ALP activity, alizarin red-S staining experiment, and Western blotting experiment. RNX performed all the RT-qPCR analyses, WJH participated in the bioinformatics analysis. SYZ wrote and revised the manuscript. All authors have read and approved the final manuscript.

Acknowledgements

Not applicable

Data Availability

The datasets generated and/or analyzed during the current study are available in the Gene Expression Omnibus repository, [https://www.ncbi.nlm.nih. gov/geo/query/acc.cgi?acc=GSE 211413]

References

1. Karsenty G, Khosla S. The crosstalk between bone remodeling and energy metabolism: A translational perspective. Cell Metabol. 2022;34:805–17.
2. Artamonov MY, Sokov EL, Kornilova LE, Minenko IA. The Intraosseous Environment: Physiological Parameters, Regulatory Mechanisms, and Emerging Insights in Bone Biology. Int J Mol Sci. 2025;26:3876.
3. Baldessari C, Pipitone S, Molinaro E, et al. Bone metastases and health in prostate cancer: From pathophysiology to clinical implications. Cancers. 2023;15:1518.
4. Satcher RL, Zhang XH-F. Evolving cancer–niche interactions and therapeutic targets during bone metastasis. Nat Rev Cancer. 2022;22:85–101.
5. Pang L, Gan C, Xu J, et al. Bone metastasis of breast cancer: molecular mechanisms and therapeutic strategies. Cancers. 2022;14:5727.
6. Jiang H. Prostate cancer bone metastasis: Molecular mechanisms of tumor and bone microenvironment. Cancer Manage Res 219–37, 2025.

7. Zhang X. Interactions between cancer cells and bone microenvironment promote bone metastasis in prostate cancer. Cancer Commun. 2019;39:76.
8. Choi E, Buie J, Camacho J, Sharma P, de Riese WT. Evolution of androgen deprivation therapy (ADT) and its new emerging modalities in prostate cancer: an update for practicing urologists, clinicians and medical providers. Res Rep Urol 87–108, 2022.
9. Wells KV, Krackeler ML, Jathal MK et al. Prostate cancer and bone: clinical presentation and molecular mechanisms. Endocrine-related Cancer 30: 2023.
10. He W, Wang Z, Li Z. MicroRNAs in bone metastases: mechanisms and research progression. Front Oncol. 2025;15:1552902.
11. Jin L, Shao Z, Ye Z, Li B. Osteoblasts in bone metastasis: key players in the tumor microenvironment and therapeutic targets. Biochimica et Biophysica Acta (BBA)-Reviews on Cancer 189435, 2025.
12. De Visser KE, Joyce JA. The evolving tumor microenvironment: From cancer initiation to metastatic outgrowth. Cancer Cell. 2023;41:374–403.
13. Popper H. Primary tumor and metastasis—sectioning the different steps of the metastatic cascade. Translational lung cancer Res. 2020;9:2277.
14. Chi-Cheng M, Ao-Rong O-Y, Zi-Xian C, Shan-Chao Z, Ming-Kun C. Targeting the triad: phenotypic plasticity, tumor microenvironment and bone microenvironment in prostate cancer bone-metastatic events. Biochimica et Biophysica Acta (BBA)-Reviews on Cancer 189388, 2025.
15. Tsukasaki M, Hamada K, Okamoto K et al. LOX fails to substitute for RANKL in osteoclastogenesis. Journal 2017.
16. Sun YX, Schneider A, Jung Y, et al. Skeletal localization and neutralization of the SDF-1 (CXCL12)/CXCR4 axis blocks prostate cancer metastasis and growth in osseous sites in vivo. J Bone Miner Res. 2005;20:318–29.
17. Chen C, Wang S, Wang N, et al. Icariin inhibits prostate cancer bone metastasis and destruction via suppressing TAM/CCL5-mediated osteoclastogenesis. Phytomedicine. 2023;120:155076.
18. Chen H, Zhou L, Wu X, et al. The PI3K/AKT pathway in the pathogenesis of prostate cancer. Front Biosci (Landmark Ed). 2016;21:1084–91.
19. Abdullah K, Sharma G, Qais FA, et al. Hydroxychloroquine interaction with phosphoinositide 3-kinase modulates prostate cancer growth in bone microenvironment: In vitro and molecular dynamics based approach. Int J Biol Macromol. 2024;266:130912.
20. Miller KA, Degan S, Wang Y, et al. PTEN-regulated PI3K-p110 and AKT isoform plasticity controls metastatic prostate cancer progression. Oncogene. 2024;43:22–34.
21. Guo S, Wang S, Yuan S, et al. Construction of dynamic ceRNA regulatory networks in osteogenesis during fracture healing based on transcriptomic analysis. Sci Rep. 2025;15:26946.
22. Lian Z, Chang T, Ma S, et al. MiR-96-5p induced NDRG1 deficiency promotes prostate cancer migration and invasion through regulating the NF-κ B signaling pathway. Cancer Biomarkers. 2022;35:83–98.

23. Colden M, Dar AA, Saini S, et al. MicroRNA-466 inhibits tumor growth and bone metastasis in prostate cancer by direct regulation of osteogenic transcription factor RUNX2. Cell Death Dis. 2018;8:e2572–2572.
24. Sur S, Ray RB. Emerging role of lncRNA ELDR in development and cancer. FEBS J. 2022;289:3011–23.
25. Sur S, Nakanishi H, Steele R, Zhang D, Varvares MA, Ray RB. Long non-coding RNA ELDR enhances oral cancer growth by promoting ILF3-cyclin E1 signaling. EMBO Rep. 2020;21:EMBR202051042.
26. Liu J, Liu Z-X, Li J-J, et al. The macrophage-associated lncRNA MALR facilitates ILF3 liquid–liquid phase separation to promote HIF1α Signaling in esophageal cancer. Cancer Res. 2023;83:1476–89.
27. Maurizi A, Ponzetti M, Rucci N. How the seed prepares the soil: the bone/bone marrow pre-metastatic niche. J Cancer Metastasis Treat 2022.
28. Paskeh MDA, Entezari M, Mirzaei S, et al. Emerging role of exosomes in cancer progression and tumor microenvironment remodeling. J Hematol Oncol. 2022;15:83.
29. Ahmad M, Weiswald L-B, Poulain L, Denoyelle C, Meryet-Figuiere M. Involvement of lncRNAs in cancer cells migration, invasion and metastasis: cytoskeleton and ECM crosstalk. J Experimental Clin Cancer Res. 2023;42:173.
30. Abate-Shen C, Nunes de Almeida F. Establishment of the LNCaP cell line–the dawn of an era for prostate cancer research. Cancer Res. 2022;82:1689–91.
31. Bousch JF, Beyersdorf C, Schultz K, Schnitker M, Suschek CV, Maus U. Comparison of Primary Human Osteoblast-like Cells and hFOB 1.19 Cells: Contrasting Effects of Proinflammatory Cytokines. Cells. 2025;14:1264.

Figures

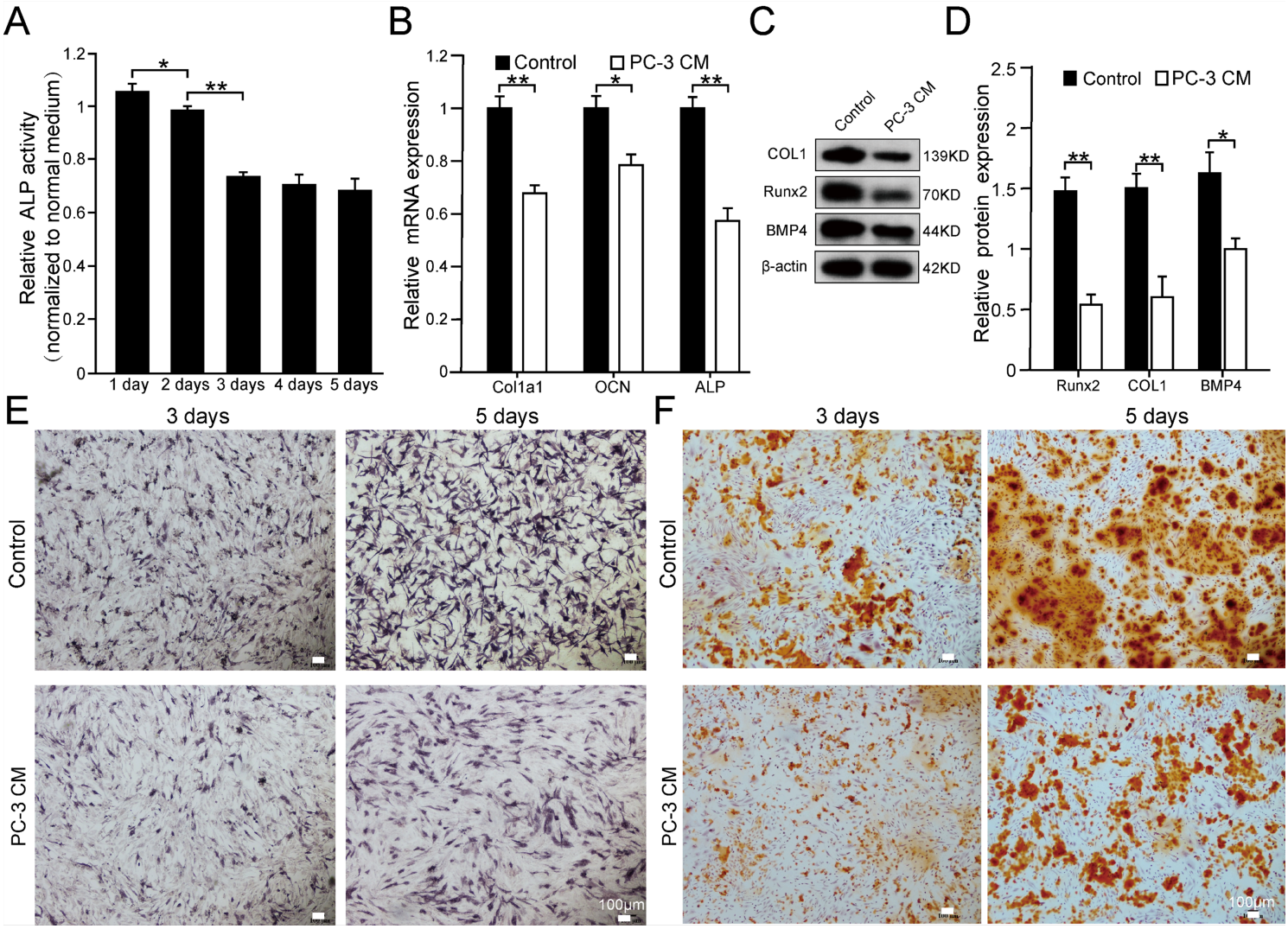


Figure 1

Assay of osteoblastic differentiation of MC3T3-E1 cells treated with PC-3 CM. MC3T3-E1 cells cultured with PC-3 CM decreased the MC3T3-E1 cells ALP activity (A, E), decreased the mRNA levels of Runx2, Col I, and BMP4 (B), decreased Runx2 Col I, and BMP4 protein levels (C-D), and reduced calcium deposition of the cells (F)

*p< 0.05 and **P<0.01, compared with the control group.

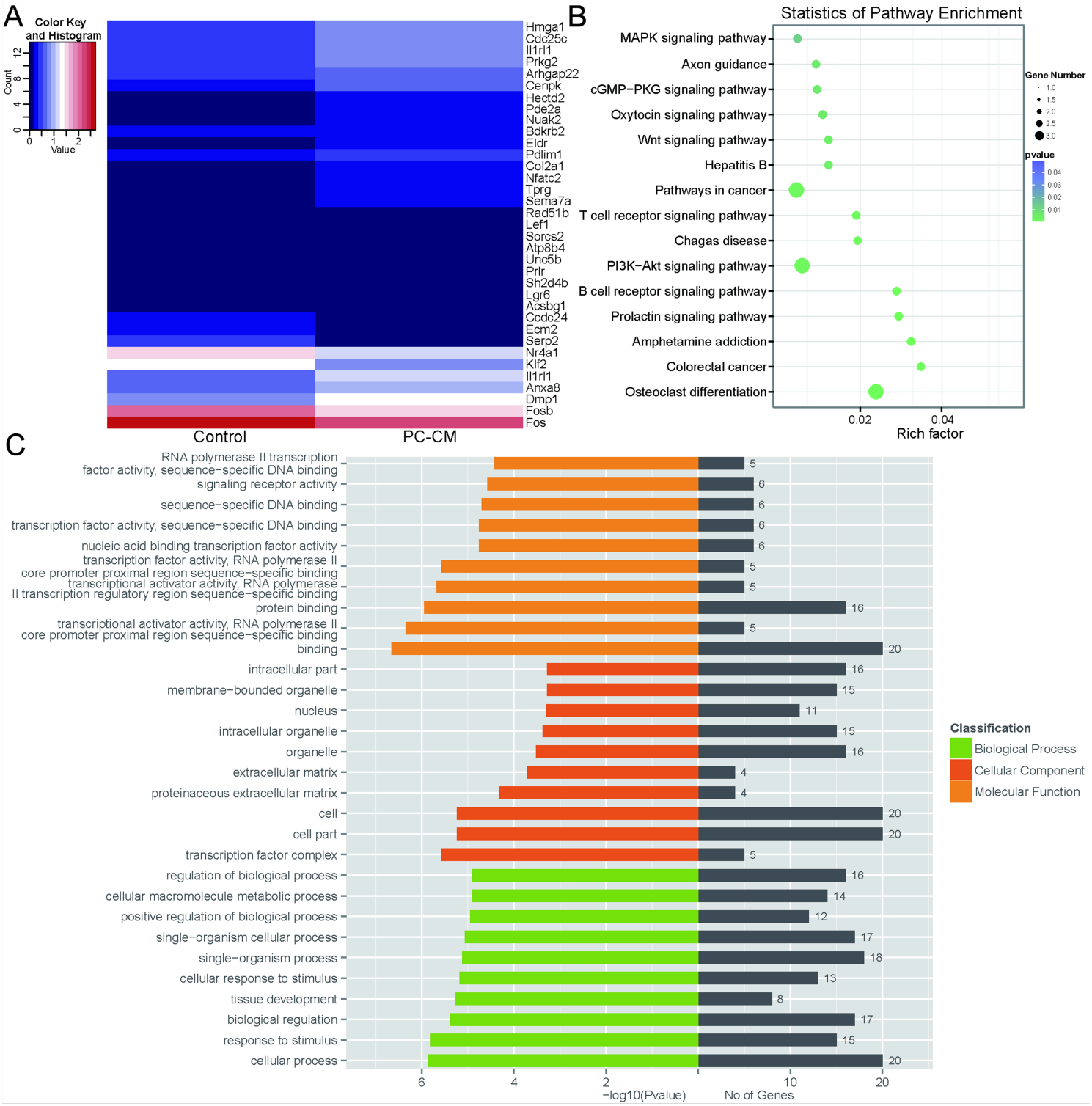


Figure 2

The differentially expressed mRNAs from MC3T3-E1 cells treated with PC-3 CM. (A) Heatmap of differentially expressed gene. (B) The most significant KEGG pathway enriched on DEGs. (C) The most significant GO enriched terms on DEGs.

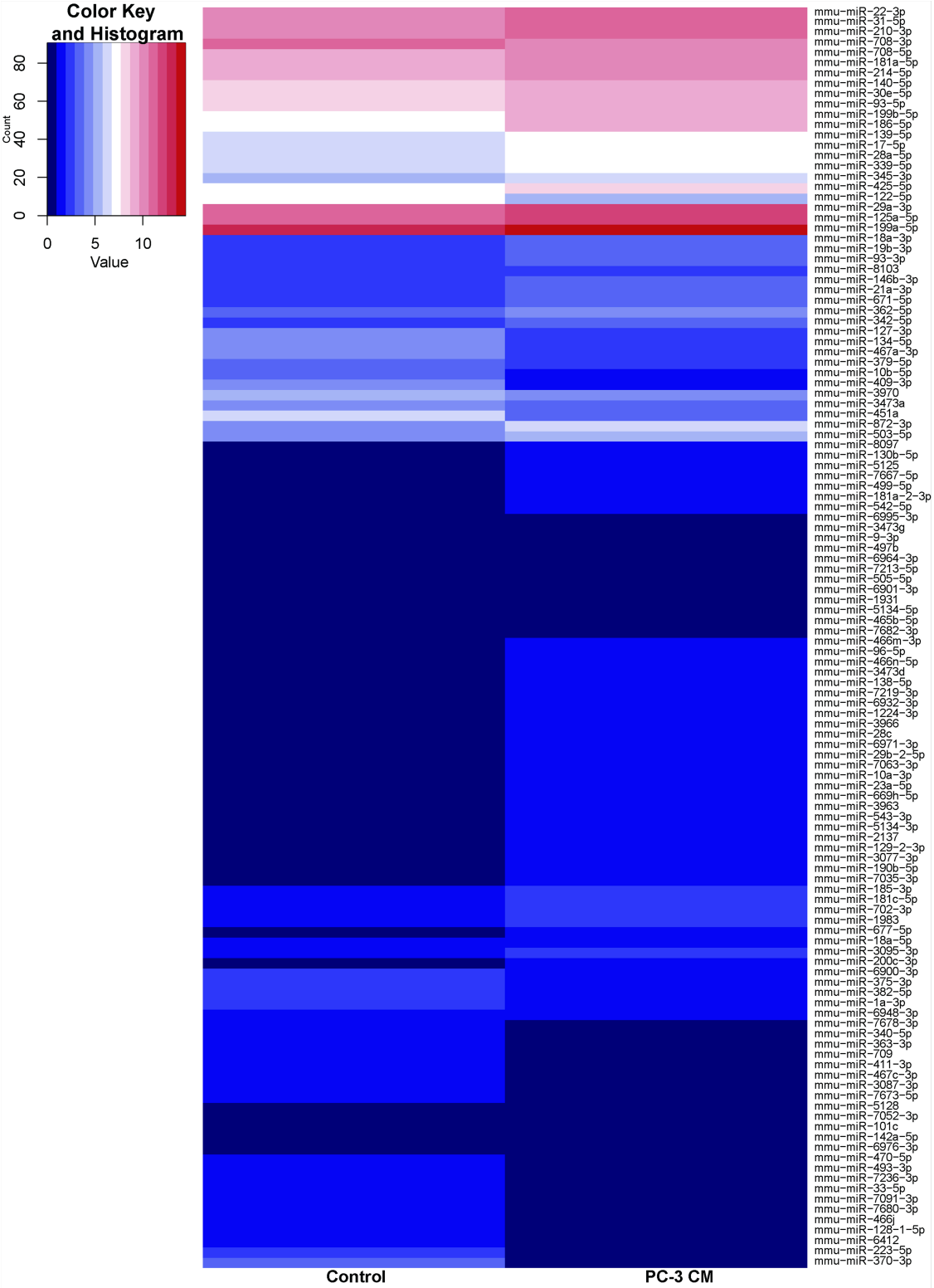


Figure 3

Differentially expressed miRNAs from MC3T3-E1 cells treated with PC-3 CM, were showed with heatmap.

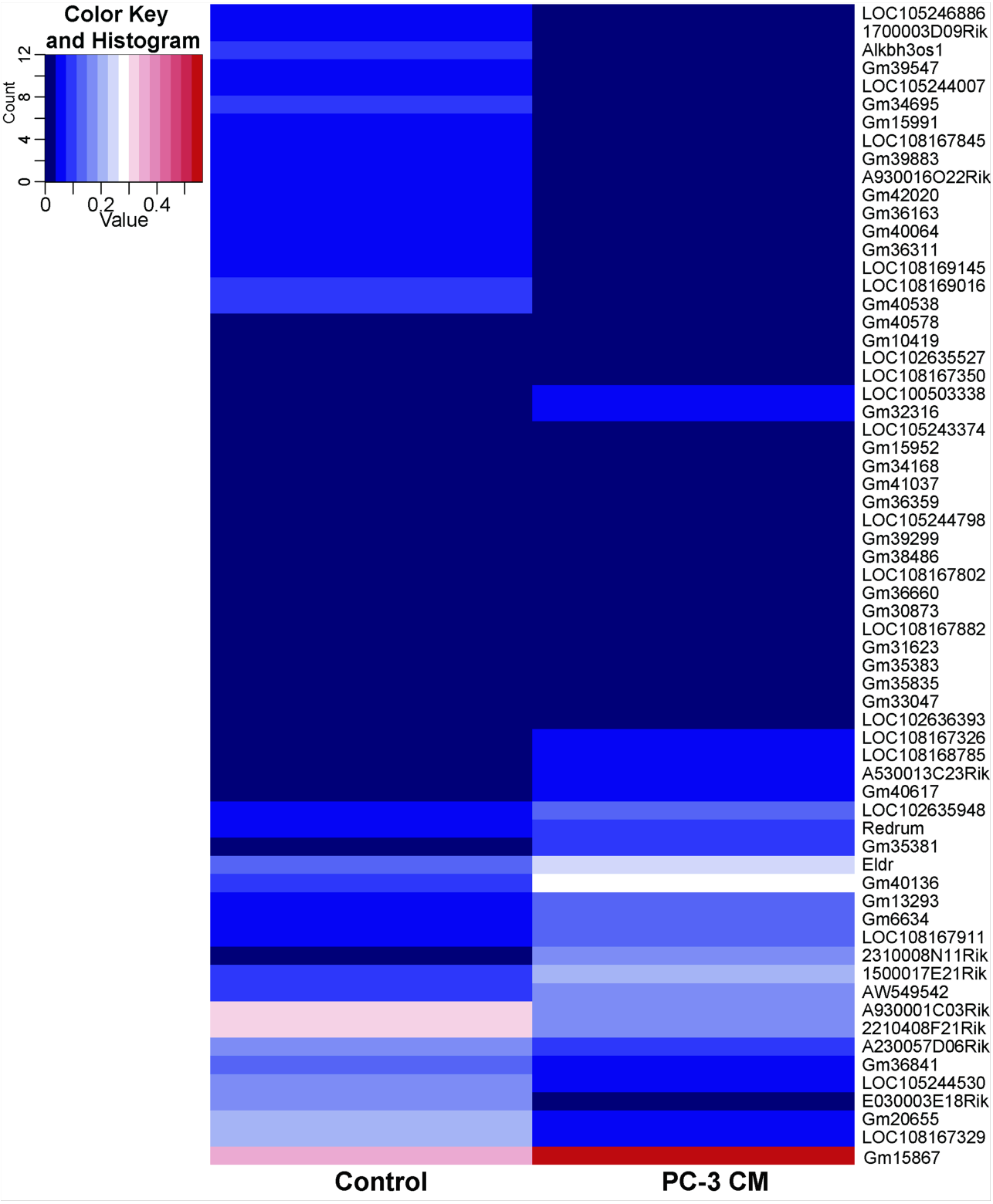


Figure 4

Differentially expressed lncRNAs from MC3T3-E1 cells treated with PC-3 CM, were showed with heatmap.

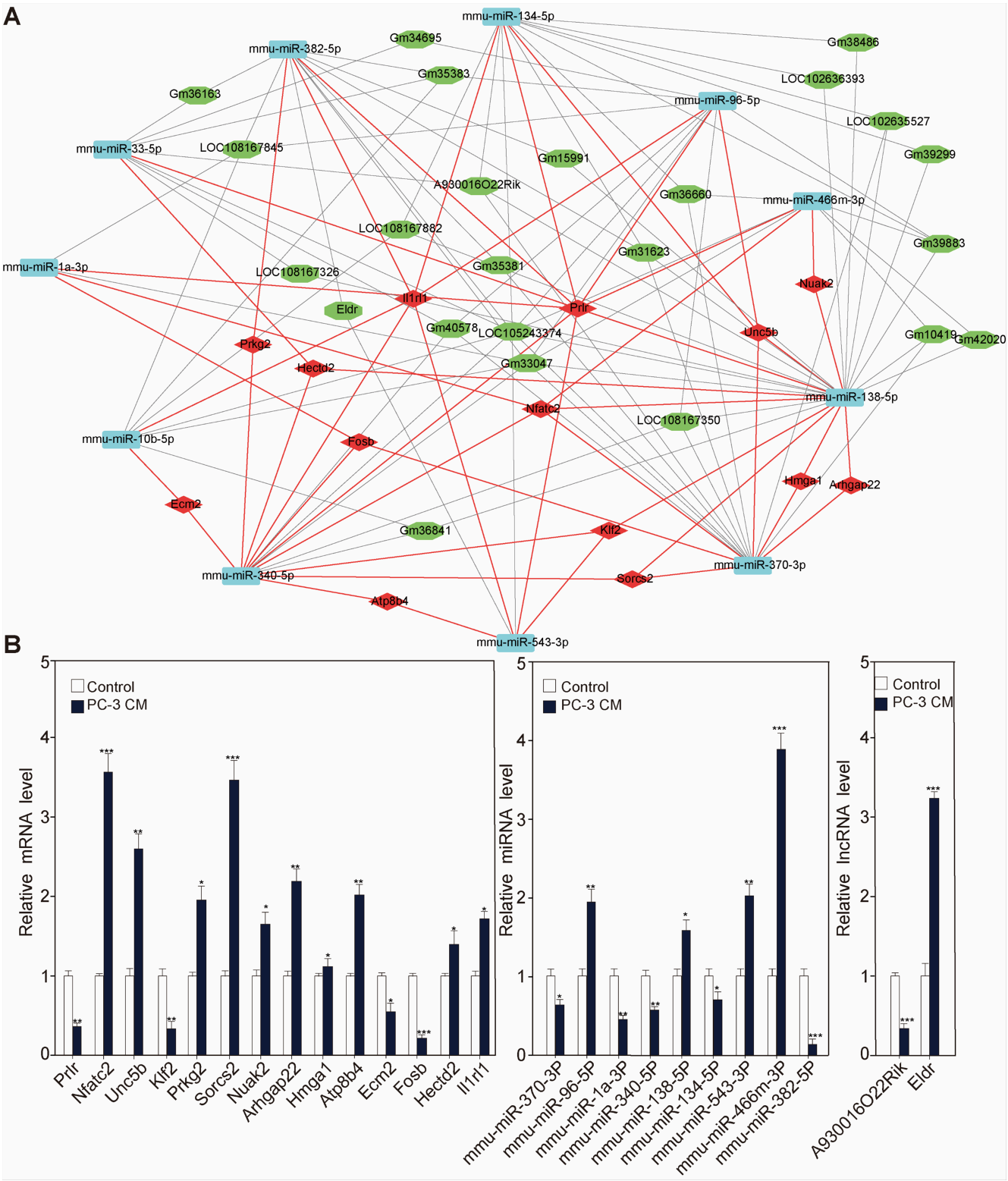


Figure 5

The construction and validation of CeRNA regulatory networks. (A) The construction of CeRNA regulatory networks. The red oval represents mRNAs, the green rhombus represents miRNAs, the blue oval represents LncRNAs. (B) The differential expression levels of mRNAs, miRNAs, and lncRNAs were verified using RT-qPCR.